Drivers of landscape evolution in eastern Tibet

Drivers of landscape evolution in eastern Tibet

Luobin Yan[1], Mikael Attal[2], Simon M. Mudd[2], Ke Zhang[3] Yuntao Tian[3]

（1. School of geographical sciences, Southwest University, Chongqing 400715;

（2. School of Geosciences, University of Edinburgh;

（3. School of earth sciences and engineering, Sun Yat-sen University.）

Abstract: The eastern margin of the Tibetan Plateau is characterized by two end-member morphologies: 2-3-km-deep canyons that are juxtaposed against extensive high elevation, low relief landscapes. Past researchers have highlighted topographic evidence for mobile drainage divides in this region. Active thrusting is thought to drive river gorge incision originating from the east, but within the eastern Tibetan plateau, there is no evidence for focussed thrusting, and no significant post-Cenozoic shortening structures are evident at the surface upstream of the Three Rivers regions. In this region, researchers have attributed the evident landscape transience to different mechanisms, including upward propagation of an incision signal, regional uplift, and local uplift caused by strike-slip motion. Here, we quantify topographic metrics to document the geomorphic response to the proposed tectonic forcing. Specifically, we quantify channel steepness and identify knickpoints to assess evidence for landscape transience and potential accelerated incision triggered in eastern Tibet. We find that k_{sn} and slope systematically increase downstream along the Tongtianhe River (TR) which bisects the study area from NW to SE and is part of the Yangtze River system, but not along adjacent main stem rivers with similar orientation, therefore ruling out the effect of a regional uplift gradient. The spatial distribution of knickpoints does not cluster along or around fault lines, which we interpret to mean that local faulting is not likely a significant factor causing the systematic variations in the topographic metrics. We find that tributaries of the TR exhibit large non-lithological channel convexities, and that the elevation of these knickpoints above the tributaries' mouth increases towards the SE, in the TR's downstream direction. This observation can be best explained by a transient signal propagating upstream along the TR. An additional large non-lithological knickpoint along the TR, as well as a strong local drainage divide disequilibrium between the TR's tributaries and adjacent basins, suggest that waves of incision, potentially set by regional uplift, are propagating up the TR but not up the adjacent major river systems (the Mekong and eastern branch of Yangtze rivers). We propose these waves of incision are the first-order driving force for river arrangements in eastern Tibet. Accordingly, we reconstruct the evolution processes of landscapes in eastern Tibet.

Keywords: River capture; River networks reorganization; Eastern Tibet; Chi analysis

1 Introduction

The shape of the Earth's surface is mainly determined by the competition between tectonic motion and Earth surface processes. Because the response time of river systems to perturbations is on the order of millions of years (Whipple, 2001; Whipple and Tucker, 1999; Whittaker and Boulton, 2012; Willett et al., 2014), landscapes are far from equilibrium in many settings. Many landscapes exhibit river channel steepening, headward erosion, drainage divide migration and river capture (Fan et al., 2018). Beyond landscape morphology, such drainage reorganization processes have been shown to affect ecology (Gallen, 2018; Ott, 2020) and river ecosystems (Albert et al., 2018; Gallen, 2018; Lyons et al., 2020; Souza et al., 2020; Swartz et al., 2007; Waters et al., 2020; Willett et al., 2014). For instance, the presence of the Tibetan Plateau is thought to profoundly influence biodiversity in Asia (Deng et al., 2020; Spicer, 2017). Understanding the land surface dynamics of the Tibetan Plateau, which is the most extensive elevated surface on Earth, is critical for exploring the links between morphology and other components of the Earth system. The central plateau is internally drained, which contrasts sharply with the plateau's steep and active eastern margin, where three of the world's largest rivers (Salween, Mekong and Yangtze) are incising at ~0.3 to 0.4 mm/year (Clark et al., 2005; Ouimet, 2007). In addition, the unique geomorphology of eastern Tibet, as well as its unique aquatic plants, plankton, benthic animals, and fish (Pan et al., 2013), testify to a highly dynamic history over the last few million years.

As the headwaters of the 'Three Rivers' (Salween, Lancangjiang River, Yangtze) region, eastern Tibet is the topographic transition zone connecting bedrock river gorges up to 3 km deep (Yang et al., 2015) and high-elevation, low-relief landscapes with low erosion rates (Duvall et al., 2004; Henck et al., 2011; Ouimet et al., 2009; Wilson and Fowler, 2011). Farther west and away from the Three Rivers region, the events leading to and the drivers of the development of modern topography are less clear. One such region is the Qiangtang terrane (Figure 1-a), the eastern component of which features steep canyons inset into a mosaic of spatially extensive high elevation, low-relief landscapes (Figure 1-a). Some authors have argued that this morphology is caused by incision into a uniform elevated pre-existing low-relief landscape (Clark et al., 2006; Whipple et al., 2017a; Yuan et al., 2022), whereas others claim its origin is due to river network reorganization driven by tectonic deformation, a process that might leave remnants of the original network isolated and starved of drainage area (Yang et al., 2015). Towards the Three Rivers region, active thrust faulting is thought to drive channel incision (Clark et al., 2004; Clark et al., 2005; Ou et al., 2021), but to

63 the east, the contrasting gorges and low relief surfaces are not co-located with major faults (Whipple et al.,
64 2017). One hypothesis is that this morphology is driven by channel incision signals propagating upstream
65 from the tectonically active region (Harkins et al., 2007; Fan et al., 2021), which we aim to test in this study,
66 as detailed below.

67 The uplift of Tibet involves a series of collisional events of several Gondwanan terranes with Asia and
68 the final accretion of the Indian subcontinent (Molnar and Tapponnier, 1975; Yin and Harrison, 2000; van
69 Hinsbergen et al., 2012). Since the India/Eurasia collision, ~2000 km of shortening has occurred in the
70 Tibetan Plateau, which is thought to have been absorbed by underthrusting of the Indian lithosphere,
71 shortening of the Himalayan thrust belt, and shortening via thrusting and strike-slip faulting in the plateau
72 interior (e.g., Kapp and DeCelles, 2019). The continued convergence resulted in the outward and upward
73 growth of the Tibetan Plateau through crustal shortening and/or lower crustal flow during the Neogene
74 (Tapponnier et al., 2001; Clark et al., 2005; Molnar, 2005; Royden et al., 2008; Tian et al., 2015).

75 All studies agree that eastern Tibet has experienced a period of substantial tectonic uplift, but there is
76 debate over the timing. Early authors suggested, based on fission-track dating, that uplift accelerated at 3.6
77 Ma (Li et al., 1996). Thermochronometric data suggest a late Miocene (at ~10Ma) increase of river incision,
78 which has been interpreted as evidence of coeval rock and surface uplift (Clark et al., 2005; Ouimet et al.,
79 2010; Tian et al., 2018). Recent thermochronological studies suggest the occurrence of early Miocene (Tian
80 et al., 2014), middle Miocene (Nie et al., 2018), Oligocene and earlier phases of rock exhumation (Wang et
81 al., 2012; Shen et al., 2016; Zhang et al., 2022), indicating a spatially and temporally heterogeneous rock
82 uplift pattern (Tian et al., 2014; Zhang et al., 2022; Wang et al., 2008). Duvall et al. (2012) inferred broad
83 surface uplift as the main driver of the widespread late Cenozoic increase in erosion rates across the interior
84 of eastern Tibet. Meanwhile, Henck et al. (2011) noted an exhumation gradient changing from 0.01 to 8
85 mm/yr from west to east of eastern Tibet, suggesting a long-wavelength rock uplift pattern. Recent research
86 has also attempted to link the rapid incision of the major rivers to the intensification of monsoon rainfall
87 (Nie et al., 2018). All these studies point towards accelerated uplift in eastern Tibet driving channel incision
88 that originates in the east and then propagates upstream.

89 Drainage divide migration is a common feature of tectonically active, transient landscapes. In these
90 landscapes, divides tend to migrate towards the side with a higher uplift rate, with a lower erosion rate, in
91 the direction of horizontal advection/shortening (Bonnet, 2009; He et al., 2021; Willett et al., 2014), and/or

towards stronger, less erodible rocks (Giachetta et al., 2014; Strong et al., 2019; Zondervan et al., 2020b). Topographic evidence for divide migration has been reported in this region (Whipple et al., 2017a; Yang et al., 2015). However, while the surface of eastern Tibet appears uplifted, no significant Cenozoic shortening structures are evident at the surface (Burchfiel et al., 1995; Clark et al., 2004; Clark et al., 2006; Royden et al., 1997; Studnicki-Gizbert et al., 2008; Wang and Burchfiel, 2000). Is the divide migration in this region caused by propagating knickpoints from further downstream, a regional uplift gradient (Henck et al., 2011), or strike-slip faulting in the region (Yu, Wang et al. 2018)? Each of these potential scenarios should lead to distinct and testable regional morphological patterns, including: regional gradient of channel steepness reflecting uplift gradient (Kirby and Whipple 2012), wave-like main stem and tributary steepening associated with the upstream propagation of uplift signals (Binnie et al., 2007; Gallen et al., 2011), or local disequilibrium associated with drainage reorganization due to strike-slip faulting (Yu, Wang et al. 2018). In this study, we extract channel and catchment-wide metrics, as well as the location of major knickpoints along the main rivers of the study area and their tributaries, to test whether topographic analysis can discriminate between these scenarios, and to identify the main drivers of landscape evolution in the study area.

2 Geologic and geomorphological background

Our research area is located at the junction of the Qiangtang and Songpan-Garze terranes (Figure 1-a). The western part of the area is the top surface of a plateau, with little river incision, whereas the eastern part is incised by more than 1 km (Figure 1). The existence of such a clear topographic contrast makes this area an ideal candidate to test the proposed hypotheses regarding the drivers of landscape evolution in Eastern Tibet, as each of the proposed drivers should lead to discernible topographic signals. The area is bisected by the southeast-flowing Tongtianhe River (TR), which is one of the tributaries of the Yangtze River (YZR), essentially forming the headwaters of the YZR's western branch (Figure 1-a, b). The TR is sandwiched between (i) the Yalongjiang River (YLR) and Yellow River to the NE, and (ii) the Lancangjiang River (LR) to the SE (Figure 1). The LR belongs to the Mekong River system. The YLR is a headwater tributary of the eastern branch of the YZR: while both TR and YLR belong to the YZR system, their courses connect ~1000 km downstream (Figure 1-a).

120 The surface lithology of the area is mainly composed of strongly folded Triassic siliciclastic rock. The
121 northern part of the TR is mostly siliciclastic sedimentary rocks and the southern part is mixed sedimentary
122 rocks (including mixed carbonate-siliciclastic sediment, but carbonates are not dominant). Unconsolidated
123 sediments are only found along the river channel of the YLR and upper mainstem reaches of the TR.
124 Plutonics are only sporadically distributed, and pyroclastics are concentrated in the upper reaches of LR. In
125 addition, the area of glaciers is small: glaciers are only present around the divide between the TR and
126 headwaters of the LR (Figure 1-c).

127 Crustal shortening in the Qiangtang and Songpan-Garze terranes mostly occurred before the Oligocene,
128 as shown by the formation and folding of several foreland basins (Spurlin et al., 2005). Oligocene and
129 subsequent deformation is mainly dominated by SE-striking Garzi-Yushu strike-slip fault (Wang et al. 2008).

130 Our research area is affected by the northwestern part of the Ganzi-Yushu Fault and associated series
131 of secondary structures (Wen et al., 2003). The Ganzi-Yushu Fault is left lateral, as shown by offset
132 landforms that include beheaded stream, fault scarps, pull-apart basins and shutter ridges (Wang et al., 2008;
133 Wen et al., 1985; Zhou et al., 1997). The fault initiated in the late Miocene, with a total slip of ~80 km, as
134 documented by offsets of river trunk and the syn-tectonic ~12-Ma Gongga Shan granites (Wang et al., 2008;
135 Searle et al., 2016). The left slip is ongoing as shown by GPS observations (Taylor and Yin, 2009) and large
136 earthquakes (such as the Ms 7.1 Yushu earthquake, 2010).

137 Due to the activity of the Ganzi-Yushu Fault, river capture and flow reversal are widespread on the
138 north side of the TR (Barbour, 1936; Li et al., 2013b; Yu et al., 2018). Whilst unusual river patterns (e.g.,
139 tributaries joining larger channels at oblique angles) and inferred captures have been identified in these
140 studies, their importance in driving the geomorphological evolution of the area compared to the other drivers
141 remains unknown.

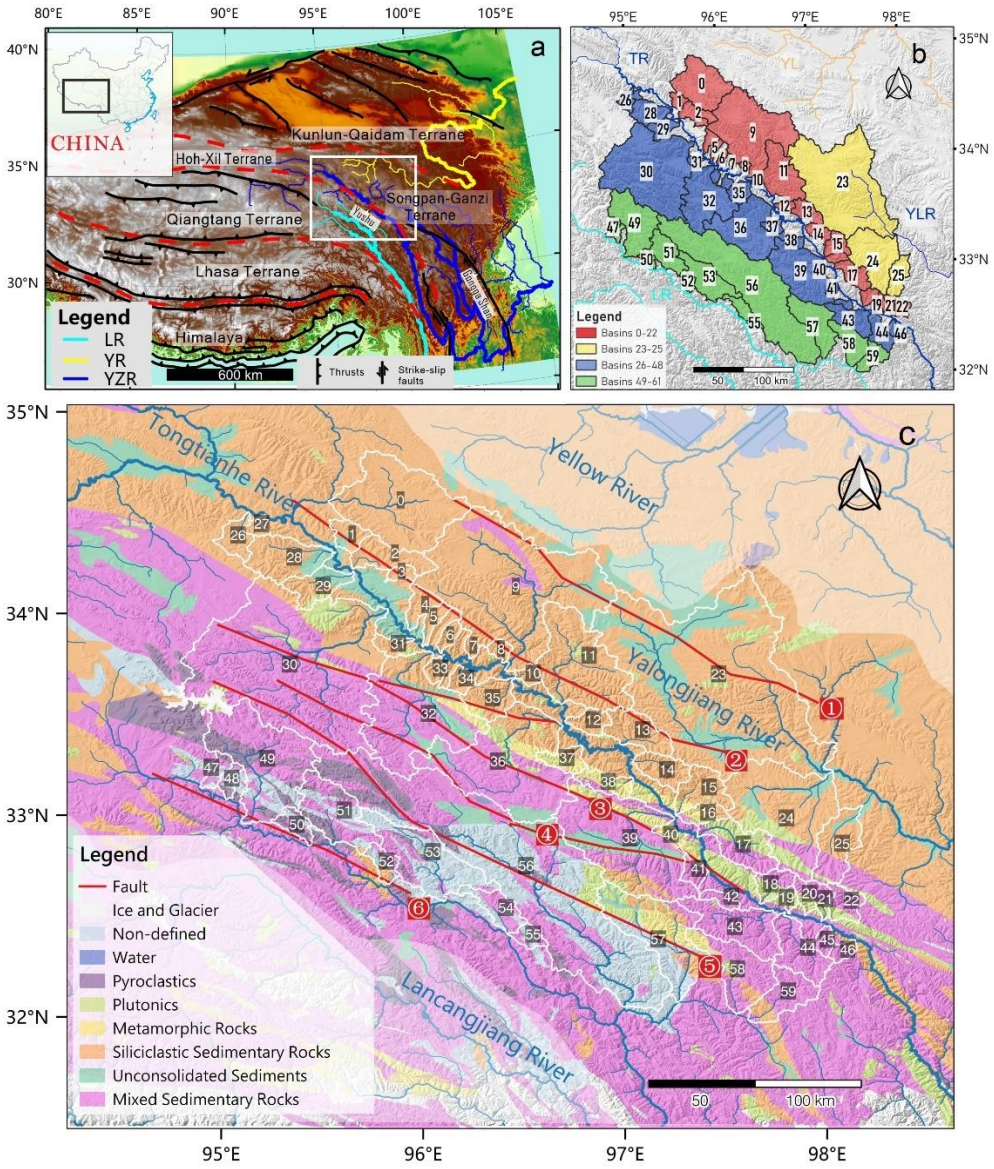

Figure 1. Map of the Tibetan region showing the principal terranes, strike-slip faults and the location of study area. The fault information (belts and major faults) is adapted from the active structural map of China (Deng, 2007). (a) Topographic map of Tibet showing the main faults and terranes, as well as the three major rivers in this area: the Yangtze River (YZR), the Lancangjiang River (LR), and the Yellow River (YR). White rectangle shows location of the study area shown in (b) and (c). (b) Hillshade of the study area, with study catchments delimited and numbered. Colours indicate which drainage system the catchments belong to: green for the Lancangjiang River (LR - part of the Mekong River system), yellow for the Yalongjiang River (YLR, part of the YZR's eastern branch), and red and blue for the Tongtianhe River (TR, part of the YZR's western branch). (c) Geological map of the study area. The main faults are ①: Wudaoliang-Changshagongma Fault; ②: Wudaoliang-Qumalai Fault; ③: Ganzi-Yushu Fault; ④: Wulanwulahu-Yushu Fault; ⑤: Xiaosuben-Xialaxiu Fault; ⑥: Zaduo Fault. Labels 0-59 denote the studied basins delineated by white lines, including the following large catchments where evidence that the main rivers have been aggressors in capture events has been reported (Yu et al., 2018): Dequ Basin (9), Zhaduohe Basin (11), Duocaiqu-Ningqiaqu (30), Dengailongqu Basin (32), Yequ Basin (36), and Batanghe Basin (39).

3 Data Sources and Methodology

3.1 Data sources

We use ALOS World3D (https://portal.opentopography.org/datasets) 30 m resolution topographic

datasets produced from 2006 to 2011 (Takaku et al., 2014). The merged Digital Elevation Model (DEM) covers 120,062 km^2, and 60 basins were delineated and assigned a number in the region (Figure 1-b, c). Among them, basins 0-22 and basins 26-46 drain into the TR's mainstream from its south and north side, respectively, whereas basins 23-25 and 47-59 are within the YLR and LC catchments, respectively (Figure 1-b). The lithology data we used are from the high-resolution lithology dataset GLiM (Hartmann and Moosdorf, 2012).

3.2 Calculation of Geomorphic Parameters

Changes in channel and hillslope steepness, relief, and the presence of knickpoints, are commonly associated with variations in erosion rates or contrasts in bedrock lithology (Kirby and Whipple, 2012). In the following we describe how we extract such information. This information will then be evaluated against geological maps in order to determine whether the observed changes reflect (1) lithological changes or (2) variations in erosion rates driven by drainage reorganization, spatial variations in uplift rates, or propagating signals.

3.2.1 Calculation of the normalised steepness index k_{sn}

Authors have suggested a relationship between channel gradient and erosion rate for over a hundred years (Gilbert, 1877). Channel gradient, however, is sensitive to discharge and its proxy drainage area. Morisawa (1962) noted a power law relationship between gradient and drainage area, which was later formalized by Flint (1974):

$$S = k_s A^{-\theta} \tag{1}$$

where the parameter k_s is defined as the steepness index, and θ is defined as the concavity index. Many scholars have found that steepness is positively correlated to erosion rate (Cyr et al., 2010; DiBiase et al., 2010; Harel et al., 2016; Kirby and Whipple, 2012; Mandal et al., 2015; Ouimet et al., 2009; Safran et al., 2005; Scherler et al., 2014). The steepness index, k_s, can be determined from equation (1) (Kirby and Whipple, 2012; Snyder et al., 2000; Wobus et al., 2006). However, this method is limited by the inherently noisy data and the fact that k_s strongly depends on the value of the concavity index θ. Perron and Royden (2013) proposed a new method using elevation as the dependent variable and an integral of drainage area as the independent variable, therefore avoiding using measurements of slope：

$$z(x) = z(x_b) + \left(\frac{k_s}{A_0^{\theta}}\right) \int_{x_b}^{x} \left(\frac{A_0}{A(x)}\right)^{\theta} dx \tag{2}$$

where A_0 is an arbitrary scaling drainage area, and $z_{(b)}$ is the elevation where integration starts. According to equation (2), we can define χ as a length unit:

$$\chi = \int_{x_b}^{x} \left(\frac{A_0}{A(x)}\right)^{\theta} dx \quad (3)$$

From equation (2), we can derive：

$$z(x) = z(x_b) + \left(\frac{k_s}{A_0^{\theta}}\right)\chi \quad (4)$$

k_s can be calculated by calculating the slope of the river profile in χ space. We used a scaling area A_0 of 1 m^2 so that the gradient of the profile in χ-elevation space ("χ profile") is equal to the steepness index k_s. This methodology has been widely used in recent years (Clubb et al., 2020; DiBiase et al., 2010; Gailleton et al., 2021; Strong et al., 2019; Struth et al., 2019; Yang et al., 2015).

Because the steepness index, k_s, is strongly dependent on the value of the concavity index, θ, a reference value of the concavity index, θ_{ref}, is frequently used (Wobus et al., 2006). This reference concavity index allows comparison of k_{sn} values across multiple basins.

The choice of θ_{ref} must be considered with care since variations of θ within a realistic range could lead to variations in k_{sn} over several orders of magnitude, leading to potential misinterpretation in terms of spatial variations in erosion rates and/or their drivers (tectonics or lithology) (Gailleton et al., 2021). In this contribution, we followed the new χ-based methodology (*chi*-disorder method) of Hergarten et al. (2016) to derive the best fit θ value of all basins, as Mudd et al. (2018) showed it was as reliable and more computationally efficient than other proposed methods. The mean of all basins' concavity was used to calculate k_{sn} within each basin using the statistical technique developed by Mudd et al. (2014), which segments a χ profile into multiple contiguous segments of varied length and steepness, assesses the fit of a multitude of combinations, and identifies the best one.

3.3.2 Calculation of catchment-averaged slope

Hillslope steepness or relief have been shown to adjust to channel incision and the associated base-level fall (Ouimet et al., 2009). However, the nonlinear relationship between sediment fluxes and hillslope gradient in high-relief landscapes hinders the prediction of erosion rate using hillslope gradient (DiBiase et al., 2010; Roering et al., 1999; Roering et al., 2001; Roering et al., 2007). In our study area, the contrast between low-relief landscapes and steepened incised reaches means that maps of hillslope gradients and

median values in tributary catchments can still provide useful information regarding the relative distribution of erosion rates across the study area and its potential drivers. We therefore calculate hillslope gradient for each of the study catchments.

3.2.3 Knickpoint analysis

Abrupt changes in channel gradient or steps in elevation along river profiles are generally thought to reflect changes in either lithology or erosion rate. These topographic features are collectively called knickpoints: changes in channel gradient are called slope-break knickpoints and abrupt changes in channel elevation without a change in gradient are called vertical step knickpoints (Wobus et al., 2006).

Lithological knickpoints tend to be located at lithological boundaries, although they can in some circumstances persist after the disappearance of the contact through erosion (e.g., Strong et al., 2019). Knickpoints can also cluster along a fault when the fault separates blocks uplifting at different rates, with the river steepening over the area uplifting the fastest. These two types of knickpoints can be identified by matching their location with the known location of mapped lithological contacts and active faults. This approach can help distinguish between such knickpoints and those that represent signals of changing erosion rates associated with changes in the rate of base-level fall. Knickpoints of this latter type propagate upstream. They can reveal information on landscape evolution and erosion patterns in tectonically active regions, and their spatial distribution can provide information on the onset and nature of a tectonic event (Bishop et al., 2005; Crosby and Whipple, 2006; Liu et al., 2020). In this paper, we identify knickpoints using the reproducible method described by (Gailleton et al., 2019).

The magnitude of slope-break knickpoints ($\triangle k_{sn}$) is determined by the change in normalized channel steepness index (k_{sn}) across the knickpoint; its value can be positive or negative. Positive and negative knickpoints are defined as slope-break knickpoints where steepness decreases or increases downstream, respectively. We report the location and magnitude of the slope-break knickpoints with magnitudes less than the 1st percentile (these are highly negative, and represent the "lip" of a knickzone) and those with magnitude greater than the 99th percentile (these are at the downstream "toe" of a knickzone).

Vertical-step knickpoints are where there is a break in elevation upstream and downstream of the knickpoint but not necessarily a change in k_{sn}. We record vertical-step knickpoints that have magnitudes ($\triangle Z_{kp}$) that are greater than the 99th percentile for all vertical-step knickpoints. We also plot the location of the slope-break knickpoints with the largest and smallest $\triangle k_{sn}$ and of the vertical step knickpoints with the

243 largest drop in elevation $\triangle Z_{kp}$ along each tributary and the trunk channel.

244 4 Results

245 4.1 Spatial distribution of θ and k_{sn}

246 We compute the best fit concavity indices in sub-basins draining to major rivers in our study area
247 (Figure 2-a, b). Basins 0-22 drain to the north side of the Tongtianhe River (TR), basins 27-46 drain the
248 south side of this river, and basins 47-59 drain the north side of the Lancanjiang River (LR) (Figure 2-c).
249 Increasing basin numbers in each of these segments correspond to increasing distances downstream. The
250 distance at which each basin connects to the main stream is calculated for each dataset, with distance 0 km
251 representing the location of the upstream-most tributary junction. Note that Yu et al. (2018) suggest that
252 some of these basins may have been aggressors in drainage capture events (our basin numbers 9, 11, 30, 32,
253 36, and 39).

254 Basins draining the north side of the TR and the north side of the LR have no significant trend of
255 increasing concavity index downstream (red and green in Figure 2; as Mann-Kendall: *p*-value of 0.092 and
256 0.039, with a coefficient value of 0.229 and 0.332, respectively) (Figure 2-d, f). The basins draining the
257 south side of the TR show a significant trend with increasing distance along the TR trunk (blue in Figure 2-
258 c, as Mann-Kendall: p-value of 1.9×10^{-4}, with a coefficient value of 0.624) (Figure2-e).

259

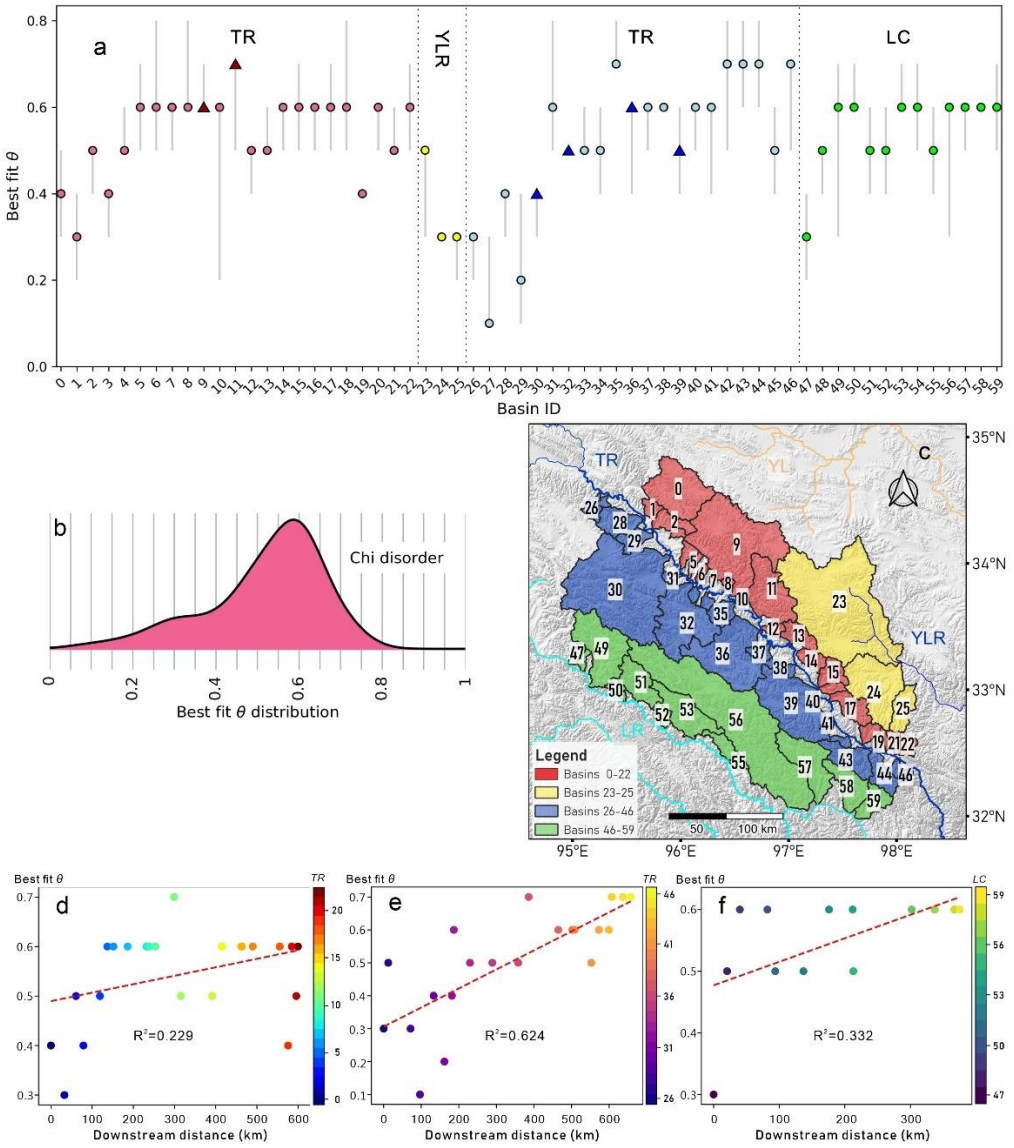

Figure 2. (a) Variation in θ using the method developed by Mudd et al., (2018). Basins are organized as follows: red (0-22) are north side tributaries of TR (number increasing in the downstream, SE direction); blue (26-46) are south side tributaries of TR (number increasing in the downstream, SE direction); green (47-59) are north side tributaries of LR (number increasing in the downstream, SE direction). Dark red and dark blue triangles are basins that may have been aggressors in capture events along the TR, as suggested by (Yu et al., 2018). The gray error bars represents the estimate of the error on the best-fit θ. (b) Distribution of θ for all basins using the *chi* disorder method of (Mudd et al., 2018). (c) Map showing the basins' numbering. (d, e and f) Trend of concavity with increasing distance downstream along TR north side, TR south side and LR, respectively.

To calculate k_{sn} for the whole region, we adopted the mean concavity value of 0.52±0.13 using the *chi* disorder method (±1 Median Absolute Deviation) (Figure 2-b). The map of normalized steepness indices (Figure 3) shows that the small basins along the TR have increasing values of k_{sn} in the TR's downstream direction (towards the SE). Except for basin 30, the steepness of large basins on the south side of the TR is higher in their downstream section, near their outlet (where they join the TR); the upper catchments exhibit

comparatively low steepness. This is confirmed by the river profiles where profiles of large basins (e.g., 36, 39) show high k_{sn} in their lower parts and low k_{sn} in the their upstream parts (Supplementary Figure 1). χ profiles of small basins are broadly linear in χ coordinates, compared to the convex-up shape of large basins.

We observe stark contrasts in cross-divide k_{sn} between catchments draining into the TR and those draining into the YLR, as highlighted by the red box in Figure 3. This trend is observed overall, with channels draining to the TR (Basin 15, 16, 17, 18, 20) significantly steeper than those draining to the YR (Basin 23-25) (Supplementary Figure 1).

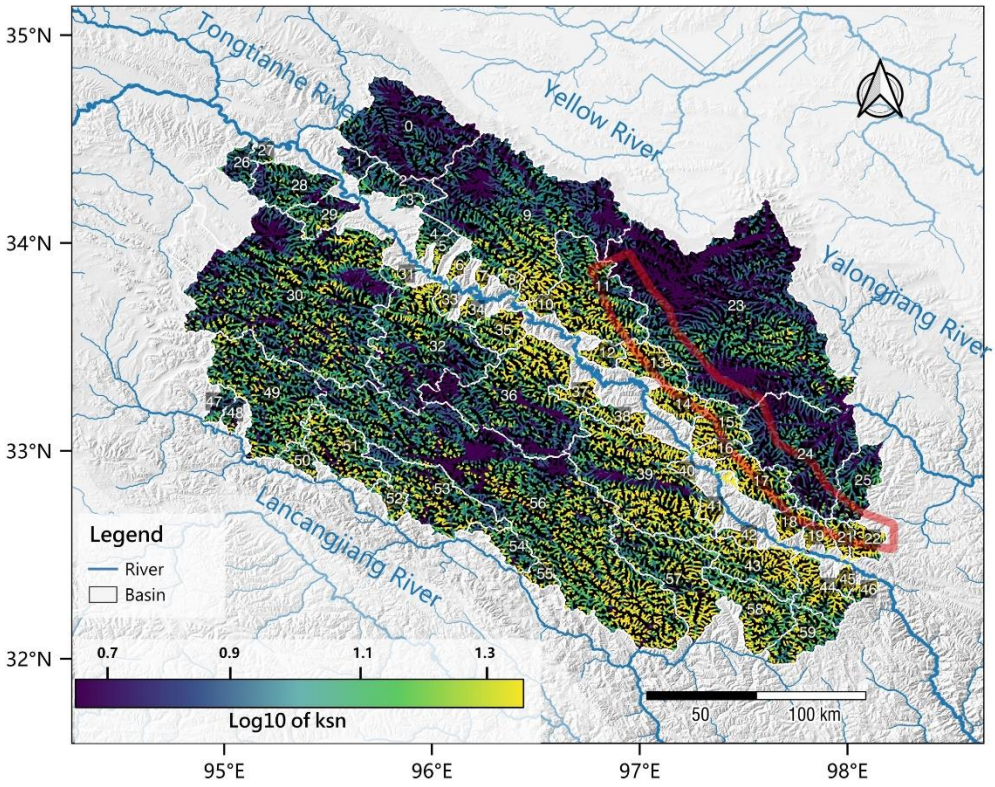

Figure 3. Map of the normalized steepness index, k_{sn}, for 60 basins. Red box highlights strong across-divide contrast in k_{sn}.

Analysis of basin-averaged k_{sn} and slope, as well as 16th and 84th percentiles (Figure 4), shows that the steepness of basins draining into the TR (red and blue trend) increases from NW to SE, that is, in the TR's downstream direction, as do the 16th-84th percentiles of k_{sn}. These trends are statistically significant, as demonstrated by a Mann-Kendall test, with a coefficient with distance downstream of 0.740 (p value of 2.8×10^{-6}) for the north side tributaries of the TR and 0.824 (p value of 4.8×10^{-6}) for the south side tributaries of the TR (Figure 4-c, d). It should be noted that the steepness of basins draining to the LR (green trend) is not correlated to distance downstream, with a p value of 0.1 (Figure 4-e). We highlight basins 9, 11, 30, 32,

36, 39, which have been suggested by previous researchers to have experienced drainage reorganization through capture as a result of local strike-slip faulting (Yu et al., 2018).

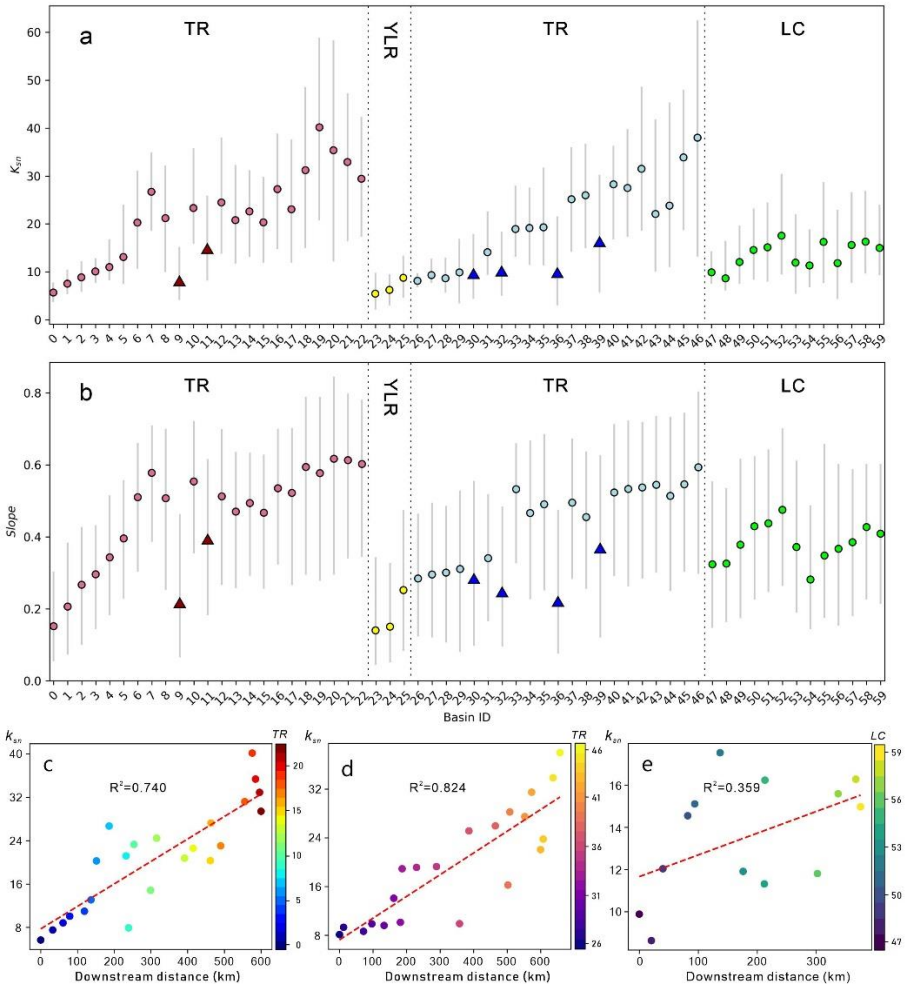

Figure 4. Median k_{sn} and slope for the 60 basins, showing variation in steepness (k_{sn}) and basin-averaged slope. (a-b) Variation in steepness as a function of basin ID. The gray bars represent the 16th and 84th percentiles of the distributions within each basin. As in Figure 2, basins are organized as follows: red (0-22) are north side tributaries of TR (number increasing in the downstream, SE direction); blue (26-46) are south side tributaries of TR (number increasing in the downstream, SE direction); green (47-59) are north side tributaries of LR (number increasing in the downstream, SE direction). Dark red and dark blue triangles are basins that previous authors have suggested have experienced drainage capture as aggressors. (c-e) k_{sn} as a function of downstream distance for TR north side, TR south side and LR, respectively. See Figure 3 for location of basins.

4.2 Spatial and vertical distribution of knickpoints

Our screening of all detected knickpoints to those with $\triangle k_{sn}$ values in the <1st and >99th percentile and $\triangle Z_{kp}$ >99th percentile resulted in the identification of 88 vertical-step knickpoints, and 90 positive and 80 negative slope-break knickpoints (Figure 5-a). To assess whether the knickpoints can be due to differential uplift along the active faults in the study area, we compute the distance between the mapped knickpoints and the mapped active faults. Knickpoints due to differential uplift along a given fault should cluster near

289 the fault. The distribution of the distance of knickpoints to the nearest fault line displays great variation.
290 The distance values for negative and positive knickpoints are higher than for stepped knickpoints. All
291 distance distributions are not centred on zero, revealing that knickpoints are not clustered along fault lines
292 (Figure 5-b).

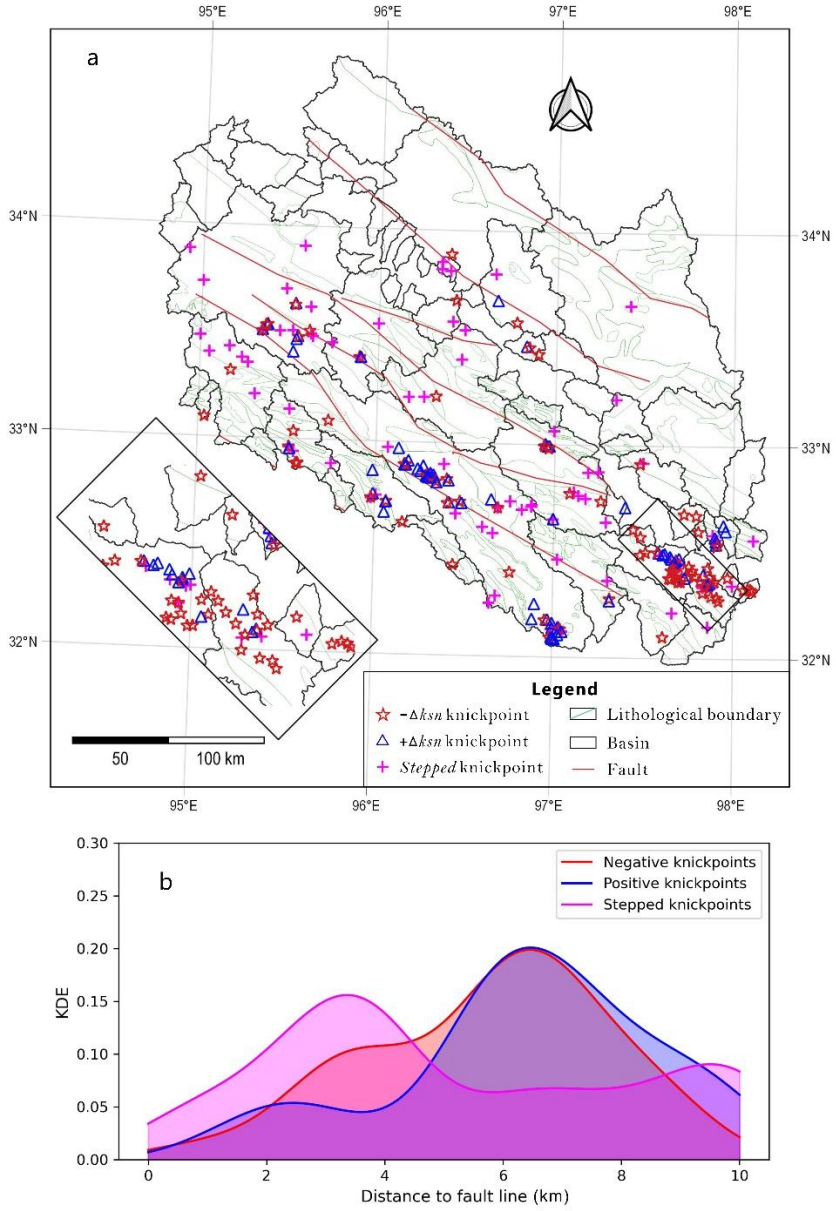

Figure 5. (a) Spatial distribution of negative, positive and vertical stepped knickpoints. (b) Distribution of distance to fault lines. Kernel density estimation (KDE) is a nonparametric representation of the probability density function. The bandwidth of the kernel smoothing window was set to 1 km.

293 We subsequently extracted the main channel in each tributary basin and extracted the knickpoints with
294 the largest values of positive and negative Δk_{sn}, as well as the largest ΔZ_{kp}, in each basin (Figure 6-a, b).

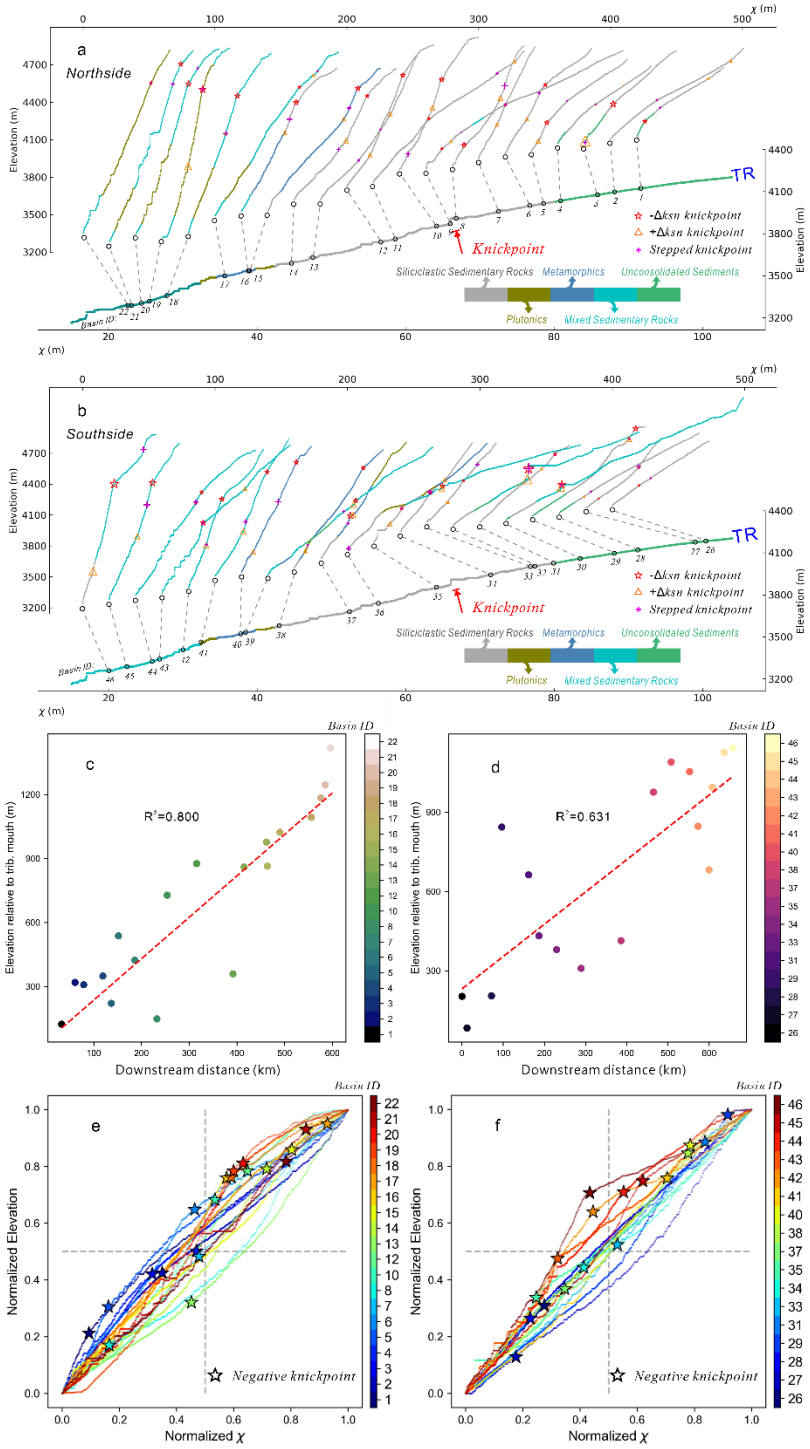

Figure 6. χ profiles of trunk channels in the TR catchment. (a-b) Spatial distribution of knickpoints in relation to lithological changes along the trunk channels. Trunk profiles of tributaries are offset by 20 m horizontally for clarity. One major knickpoint along the TR stem was well defined (Yu et al., 2021), potentially representing a transient signal propagating upstream (red arrows, see discussion). (c-d) Elevation of major non-lithological negative knickpoints above the mouth of each tributary basin as a function of distance along the TR for basins on the north and south side, respectively. (e-f) Normalized χ profiles and non-lithological negative knickpoint positions along the tributaries of the north side and south side of the TR, respectively. Colours indicate basin ID, increasing from blue to red in the SE direction (downstream). Note that the basins 9 and 11 which are hypothesized to have experienced capture as aggressors are not shown.

When not related to lithological contrasts, negative knickpoints (where k_{sn} increases downstream, that is, the upper lip of a knickzone) generally relate to a relative increase in the uplift rate: these features migrate upstream in response to changes in the rate of base-level fall (Perron and Royden, 2013; Whipple and Tucker, 1999). The position of these features may be used to infer the timing and location of base level changes (Bishop et al., 2005; Crosby and Whipple, 2006; Fan et al., 2021). We note that both the TR and its tributaries exhibit one major non-lithological negative knickpoint (Figure 6-a, b). To explore their regional significance, we plot the height of non-lithological negative knickpoints above their tributary mouth as a function of distance upstream the TR (Figure 6-c, d). We find that the height of knickpoints above tributary mouth significantly increases as one moves downstream along the TR (north side: coefficient value of 0.800, p=9.628×10^{-7}; south side: coefficient value of 0.63, p= 4.628×10^{-4}). The main knickpoint on the TR does not seem to have a major impact on these trends.

5 Discussion

5.1 Variations in concavity index

The concavity index of the studied basins within the study area varies within a narrow range, with most values around 0.5-0.6 and an average of 0.52±0.13. Global compilations of concavity indices find central tendencies around 0.45, based on both slope-area data (Tucker and Whipple, 2002) and minimization of channel distortion (Gailleton et al., 2021), which is the method used here to constrain the concavity index. Although our values are slightly higher than the central tendency of global concavity indices, they fell well within the interquartile range reported by Gailleton et al. (2021). The concavity index of basins on the south side of the TR systematically increases in the NW-SE direction, unlike that on the north side of the TR and north side of the LR which show no clear trend.

Many factors may be responsible for the changes in concavity, such as temporal or spatial variability in climate (Chen et al., 2019; Han et al., 2014; Leonard and Whipple, 2021; Whipple and Tucker, 1999), rock strength (VanLaningham et al., 2006) or uplift rate (Hurst et al., 2019; VanLaningham et al., 2006; Wickert and Schildgen, 2019). There is some topographic evidence (Hurst et al., 2019; Wickert and Schildgen, 2019), as well as theory, that suggests the concavity index decreases with increasing uplift rates (Hurst et al., 2019; Wickert and Schildgen, 2019). Some studies have found that concavity can systematically vary with lithology (Duvall et al., 2004; Lima and Flores, 2017; VanLaningham et al., 2006).

The presence of glaciers can also alter the concavity of river valleys (Brocklehurst and Whipple, 2002; Whipple et al., 1999). In this study area, glaciers only appear at the divide of basin 49 and 30 in the west of the study area (Zhang et al., 2021). However, we find that the values of concavity indices are consistent for the lower reaches of all three main channels, and that low concavities are concentrated in the basins at the highest elevations (Figure 2). It is therefore possible that these low concavity basins have experienced past glaciation. Because the driver of changing concavity indices is uncertain, we apply a single concavity index for subsequent analysis of the channel steepness index, as is standard practice.

5.2 Cause of spatial variations in channel steepness

There are clear spatial variations in the normalized steepness index across the study area. In particular, there is a clear trend of increasing k_{sn} and slope of basins that drain to the TR towards the SE, that is, in the downstream direction along the TR main stem (Figure 4-c). Mechanisms responsible for spatial variations in steepness could include: i) an uplift gradient, ii) local faulting, iii) an erosion signal propagating upstream, iv) drainage reorganization and/or v) changes in rock erodibility.

First, we explore the potential of an uplift gradient to drive spatial differences in k_{sn},. Regional uplift has been documented to drive variations in k_{sn} in a number of studies (DeLong et al., 2017; Hurst et al., 2019; Mitchell and Yanites, 2019; Struth et al., 2019; Whittaker and Boulton, 2012). In our field area, Henck et al. (2011) noted that from west to east in eastern Tibet the exhumation gradient mirrors a inferred gradient in rock uplift from 0.01 to 8 mm/yr. The increase in basin steepness observed along the TR as one moves in the SE direction is consistent with a west to east increase in rock uplift. However, if a regional gradient in tectonic uplift were used to explain the systematic variation of k_{sn}, it would be reasonable to infer that the TR and LR would experience a similar tectonic forcing and therefore exhibit a similar NW-SE trend in k_{sn}. This trend was only observed along the TR and not the LR which flows parallel to the TR (Figure 4-e). Therefore, we rule out the regional uplift gradient as a general explanation for the trends in geomorphic metrics documented in this study.

In terms of local tectonic activity, we find that slope-break knickpoints are not clustered along the active strike-slip fault lines documented in previous studies (Figure 5-b). The scattering of distances from faults implies that these strike-slip faults do not constitute boundaries between blocks uplifting at different rates and are not a major driver of channel profile geometry adjustment. This is consistent with previous work which suggests that the left-lateral strike-slip faults in the study area are only responsible for slight

vertical throw in some sections (Li et al., 2013a; Wang et al., 2008; Wen et al., 2003), implying vertical throw rates on these faults are too slow to produce knickpoints of perceivable vertical heights or k_{sn} differences. Thus, we deduce that strike-slip faults are not driving the regional increasing trend in k_{sn} and slope with increasing distance downstream, although strike-slip motion has been clearly responsible for some of the drainage reorganization documented locally (Yu, Wang et al. 2018).

In landscapes with uniform erodibility and tectonic uplift rates, one would expect channel profiles in χ-elevation space to be linear, whereas temporal increases in uplift rate would lead to convexities in transformed profiles (Perron and Royden, 2013). Figure 6-c and d show that the gradient of χ-elevation profiles for basins that drain to the TR mainstem systematically decreases from SE to NW, and that most exhibit convexities. These convexities are significant in normalized χ-elevation space for catchments on both sides of the TR (excluding basins believed to have experienced capture) (Figure 6-c), including the north side where there is no tectonic activity. These convexities are not associated with lithological boundaries, suggesting a temporal increase in relative uplift rate. Furthermore, we find that the elevation of major non-lithological negative knickpoints (i.e., where k_{sn} increases downstream) above the mouth of each tributary basin increases downstream (Figure 6-c, d). We suggest this increasing trend can be best explained by a wave of incision initiating further downstream and propagating along the TR and its tributaries: knickpoints in tributaries further SE will have had more time to propagate upstream, and will therefore be located further up their catchments (Niemann et al., 2001; Whipple and Tucker, 1999). We note a major negative knickpoint along the TR, which may represent a propagating wave of incision. However, this wave cannot be the cause of the major tributary knickpoints that we document in Figure 6-c, d, e and f, as some of these knickpoints are along tributaries that join the TR upstream of its major knickpoint. The latter may represent an additional, younger wave of incision. Its impact on the profiles of tributaries joining the TR downstream is not as noticeable, suggesting this younger wave may be smaller in magnitude than the previous one. Based on all the above observations, we propose that propagating incision signals are the first-order driving force of landscape evolution in this region of Eastern Tibet.

5.3 Mobility of catchment divides

In locations where uplift, precipitation, and lithology are spatially uniform, the river network, when in a disequilibrium state (that is, adjacent basins eroding at different rates), will adjust via divide migration or river capture until k_{sn} across divides is equal. Such phenomenon may be expected in our study area, as it

appears that incision signals are propagating along some rivers but not their neighbours. Maps of k_{sn} are a powerful tool in determining disequilibrium and scattered river capture events (Forte et al., 2016). Recently, the Gilbert metrics (i.e., cross divide contrasts in headwater elevation, relief, and gradient), originally put forward by Gilbert (1877), then formalized by Whipple (2017b), were advocated as a more robust way to interpret divide migration (Forte and Whipple, 2018). We have identified areas with high contrasts in cross-divide values of k_{sn} and Gilbert metrics distribution between the TR and YLR (Figure 7). Different lithologies on each side of the divide might cause contrasting values of k_{sn} across divides. However, we find that the lithology on both sides of the 11-15th basins and 25th basin is the same, that is, all siliciclastic sedimentary rocks. Cross-divide values of k_{sn}, in concert with Gilbert metrics, indicate the divide (red box in Figure 3) is far from equilibrium and migrating towards the YLR side, suggesting expansion of the TR catchment. A potential driver of disequilibrium is the rapid incision of a stream that is not experienced by its neighbours. We document above evidence for waves of incision propagating along the TR but not the LR. The waves of incision may be driven by a drop in base-level further downstream that affects only the western branch of the Yangtze River (to which the TR belongs) but not the Mekong River (to which the LR belongs) or the eastern branch of the Yangtze River (to which the YLR belongs) (Figure 1). Alternatively, the driver may be more regional, affecting the three river systems, but causing waves of incision propagating at different rates along the three rivers, due to differences in drainage area and/or exposed lithologies (Zondervan et al., 2020a,b). A diachronous arrival of incision waves, characterized by the early arrival of a wave of incision along the TR, could explain the observed disequilibrium.

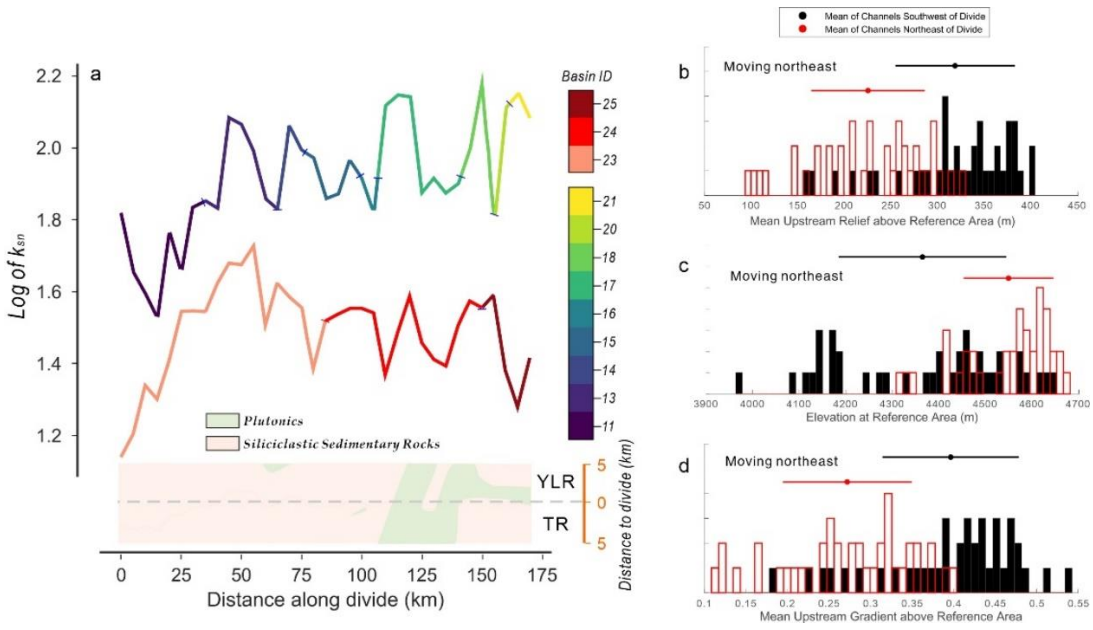

Figure 7. Value of k_{sn} along the divide and divide metrics (Gilbert metrics) in the red box of Figure 2. (a) k_{sn} is calculated for a window of 5 km across the divide between YLR and TR. The bottom panel shows the projected lithology across divide within 5 km; dashed line is the boundary between adjacent basins. k_{sn} on the YLR side is systematically lower than on the TR side. (b-d) Gilbert metrics histograms for the divide: relief upstream of, elevation at, and gradiant above reference drainage area, respectively (reference drainage area = 1×10^7 m^2). Histograms with red rectangles represent watersheds of YLR (Northeast of divide), and histograms with black fillings represent watersheds of TR (Southwest of divide). Bars above the histograms indicate median and standard deviation, and text indicates predicted direction of migration based on contrasts (all towards the NE). The radius for calculating local relief is 500 m. The results are calculated using the DivideTools (Forte and Whipple, 2018).

400

401 **5.4 Landscape evolution in the Three Rivers region**

402 We have evaluated the drivers contributing to the unique morphology of the study area. We found that
403 active faults are mostly strike-slip and have little impact, other than through local drainage organisation on
404 the south side of the TR. Lithological influence on the regional development of topography appears limited.
405 There is no evidence for an uplift gradient. The most striking feature, namely the gradient in k_{sn} in the NW-
406 SE direction observed in the tributaries of the TR (clear on NE side but potentially blurred by fault-driven
407 drainage reorganization of the SW side) but not in the adjacent basins (YLR and LR), points towards the
408 propagation of waves of incision triggered by changes in the rate of base-level lowering further downstream
409 (to the SE). Our results suggest these waves are likely the main driver of landscape evolution and regional
410 scale drainage reorganization in the study area (model in Fig. 8). The presence of this signal along the TR
411 but not adjacent river basins (reflected by trends in steepness indices and disequilibrium at drainage divides)
412 could result from a local tectonic driver affecting only the western branch of the Yangtze River, or from the
413 diachronous arrival of a more regional signal due to differences in river network structure and/or rock
414 resistance to erosion that occur downstream of our three studied river systems. Contrasts in rock resistance
415 to erosion can slow down or accelerate the propagation of signals (e.g., Zondervan et al., 2020b), leading
416 to different arrival times in adjacent basins characterized by different lithologies; such a scenario would
417 appear plausible, as terranes downstream of the study area are known to be geologically diverse (e.g., Bufe
418 et al., 2022; Roger et al., 2004).

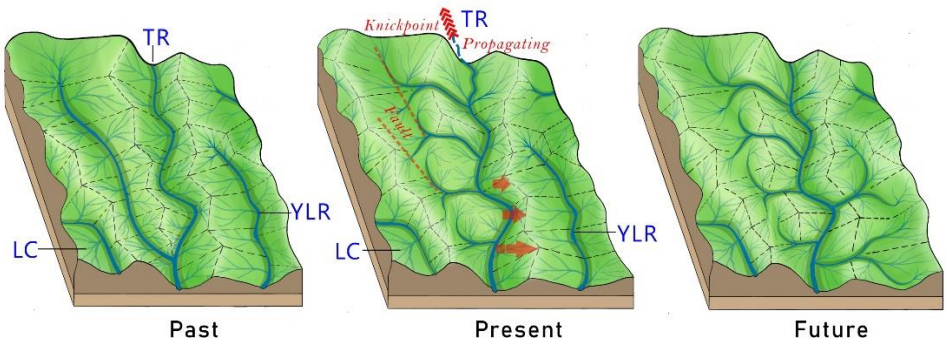

Figure 8. Summary diagram showing regime of divide migration and river captures in our study area in the Three River regions, based on our results.

6 Conclusion

Our work brings new insights into the drivers of landscape evolution in eastern Tibet. We analyzed multiple landscape metrics of basins along the Lancangjiang River, Tongtianhe River, and Yalongjiang River, which belong to the Mekong river system, western branch of the Yangtze River and eastern branch of the Yangtze River, respectively. The results of this study suggest that the first-order driving force for landscape evolution in this region is the propagation of multiple incision signals along the Tongtianhe River from further downstream (Scenario A), rather than uplift gradient (Scenario B), or strike-slip faulting (Scenario C), as proposed by other researchers.

For Scenario C, we interpret the lack of correlation between the location of faults and knickpoints as a lack of influence from strike-slip faults on the regional topographic patterns in this area, although local effects (e.g., drainage reorganization) have been reported.

For Scenario B, we rule out a regional tectonic uplift gradient because strong spatial variations in k_{sn} along the Tongtianhe River are not reflected in the Lancangjiang River which runs parallel to the Tongtianhe River.

Supporting Scenario A are the following observations. The height of knickpoints in tributaries that drain to the Tongtianhe River significantly increases towards the SE, in the Tongtianhe River's downstream direction. We cannot find a clear signal of influence from lithology on the downstream increasing trend of k_{sn} and slope along this river. This trend is therefore interpreted to record the progressive upstream propagation of incision signals originating further downstream, in the SE. The presence of this signal along the Tongtianhe River but not adjacent river basins (reflected by trends in steepness indices and

disequilibrium at drainage divides) could result from a local tectonic driver affecting only the western branch of the Yangtze River, or from the diachronous arrival of a regional signal due to differences in river network structure and/or rock resistance to erosion that would slow down or accelerate the signal in the downstream part of the three studied river systems.

Beyond eastern Tibet, this study demonstrates that upstream propagation of incision signals plays an essential role in shaping landscapes in rapidly rising rigid terranes, and likely in other tectonically active regions that experienced or are experiencing rapid uplift, in particular when these signals do not affect the area in a uniform manner, thereby driving disequilibrium. This study also demonstrates that the combination of multiple techniques of topographic analysis allows us to discriminate different scenarios that have been proposed for the evolution of the study area.

Declaration of competing interest

We declare no conflicts of interest.

Acknowledgements

L.B. Yan was supported by the National Natural Science Foundation of China (Grant No. 41901005), Fundamental Research Funds for the Central Universities (SWU 118202) and Guangdong Special Fund for National Park Construction(No: 2021GJGY026); The first author gratefully acknowledges financial support from China Scholarship Council [grant number CSC201806995083]. Software used for topographic analyses is available at https://github.com/LSDtopotools/LSDTopoTools_ChiMudd2014, with instructions available at https://lsdtopotools.github.io/LSDTT_ documentation/LSDTT_chi_analysis.html. We would like to thank Niannian Fan, Jesse Zondervan, an anonymous reviewer and Editor Martin Stokes for their helpful comments and suggestions.

References

Albert, J.S., Craig, J.M., Tagliacollo, V.A., Petry, P., 2018. Upland and lowland fishes: a test of the river capture hypothesis, in: Carina. H., Allison. P., Alexandre. AS. (Eds.), Mountains, climate and biodiversity. Wiley UK, Oxford, pp. 273-294.

Barbour, G.B., 1936. Physiographic history of the Yangtze. The Geographical Journal, 87(1), 17-32. https://doi.org/10.2307/1786198.

Binnie, S.A., Phillips, W.M., Summerfield, M.A., Fifield, L.K., 2007. Tectonic uplift, threshold hillslopes, and denudation rates in a developing mountain range. Geology, 35(8), 743-746. https://doi.org/10.1130/G23641A.1.

Bishop, P., Hoey, T.B., Jansen, J.D., Artza, I.L., 2005. Knickpoint recession rate and catchment area: the case of uplifted rivers in Eastern Scotland. Earth Surface Processes and Landforms: The Journal of the British Geomorphological Research Group, 30(6), 767-778. https://doi.org/10.1002/esp.1191.

Bonnet, S., 2009. Shrinking and splitting of drainage basins in orogenic landscapes from the migration of the main drainage divide. Nat. Geosci, 2(11), 766-771. https://doi.org/10.1038/NGEO666

Brocklehurst, S.H., Whipple, K.X., 2002. Glacial erosion and relief production in the Eastern Sierra Nevada, California. Geomorphology, 42(1-2), 1-24. https://doi.org/10.1016/S0169-555X(01)00069-1.

Bufe, A., Cook, K.L., Galy, A., Wittmann, H., Hovius, N., 2022. The effect of lithology on the relationship between denudation rate and chemical weathering pathways–evidence from the eastern Tibetan Plateau. Earth Surface Dynamics, 10(3), 513-530. https://doi.org/10.5194/esurf-10-513-2022.

Burchfiel, B.C., Zhiliang, C., Yupinc, L., Royden, L.H., 1995. Tectonics of the Longmen Shan and adjacent regions, central China. International Geology Review, 37(8), 661-735. https://doi.org/10.1080/00206819509465424.

Chen, S.A., Michaelides, K., Grieve, S., Singer, M.B., 2019. Aridity is expressed in river topography globally. Nature, 573(7775), 573-577. https://doi.org/10.1038/s41586-019-1558-8.

Clark, M., Schoenbohm, L., Royden, L., Whipple, K., Burchfiel, B., Zhang, X., Tang, W., Wang, E., Chen, L., 2004. Surface uplift, tectonics, and erosion of eastern Tibet from large‐scale drainage patterns. Tectonics, 23(1). https://doi.org/10.1029/2002TC001402.

Clark, M.K., House, M., Royden, L., Whipple, K., Burchfiel, B., Zhang, X., Tang, W., 2005. Late Cenozoic uplift of southeastern Tibet. Geology, 33(6), 525-528. https://doi.org/10.1130/G21265.1.

Clark, M.K., Royden, L., Whipple, K., Burchfiel, B., Zhang, X., Tang, W., 2006. Use of a regional, relict landscape to measure vertical deformation of the eastern Tibetan Plateau. J. Geophys Res. Earth Surf. 111(F3). https://doi.org/10.1029/2005JF000294.

Clubb, F.J., Mudd, S.M., Hurst, M.D., Grieve, S.W., 2020. Differences in channel and hillslope geometry record a migrating uplift wave at the Mendocino triple junction, California, USA. Geology, 48(2), 184-188. https://doi.org/10.1130/G46939.1.

514 Crosby, B.T., Whipple, K.X., 2006. Knickpoint initiation and distribution within fluvial networks: 236
515 waterfalls in the Waipaoa River, North Island, New Zealand. Geomorphology, 82(1-2), 16-38.
516 https://doi.org/10.1016/j.geomorph.2005.08.023.

517 Cyr, A.J., Granger, D.E., Olivetti, V., Molin, P., 2010. Quantifying rock uplift rates using channel
518 steepness and cosmogenic nuclide–determined erosion rates: Examples from northern and
519 southern Italy. Lithosphere, 2(3), 188-198. https://doi.org/10.1130/L96.1.

520 DeLong, S.B., Hilley, G.E., Prentice, C.S., Crosby, C.J., Yokelson, I.N., 2017. Geomorphology,
521 denudation rates, and stream channel profiles reveal patterns of mountain building adjacent to the
522 San Andreas fault in northern California, USA. Geol. Soc. Am. Bull. 129(5-6), 732-749.
523 https://doi.org/10.1130/B31551.1.

524 Deng, T., Wu, F., Zhou, Z., Tao, S., 2019. Tibetan Plateau: An evolutionary junction for the history of
525 modern biodiversity. Science China Earth Sciences, 2020, 63(2): 172-187.
526 https://doi.org/10.1007/s11430-019-9507-5.

527 Deng, Q., 2007. Map of Active Tectonics in China. Seismological Press, Beijing, China.

528

529 DiBiase, R.A., Whipple, K.X., Heimsath, A.M., Ouimet, W.B., 2010. Landscape form and millennial
530 erosion rates in the San Gabriel Mountains, CA. Earth Planet Sc Lett, 289(1-2), 134-144.
531 https://doi.org/10.1016/j.epsl.2009.10.036.

532 Duvall, A., Kirby, E., Burbank, D., 2004. Tectonic and lithologic controls on bedrock channel profiles
533 and processes in coastal California. J. Geophys Res. Earth Surf. 109(F3).
534 https://doi.org/10.1029/2003JF000086.

535 Duvall, A.R., Clark, M.K., Avdeev, B., Farley, K.A., Chen, Z., 2012. Widespread late Cenozoic
536 increase in erosion rates across the interior of eastern Tibet constrained by detrital low-
537 temperature thermochronometry. Tectonics, 31(3). https://doi.org/10.1029/2011TC002969.

538 Fan, N., Chu, Z., Jiang, L., Hassan, M.A., Lamb, M.P., Liu, X., 2018. Abrupt drainage basin
539 reorganization following a Pleistocene river capture. Nature communications, 9(1), 1-6.
540 https://doi.org/10.1038/s41467-018-06238-6.

541 Fan, N., Kong, P., Robl, J.C., Zhou, H., Wang, X., Jin, Z., Liu, X., 2021. Timing of river capture in
542 major Yangtze River tributaries: Insights from sediment provenance and morphometric indices.
543 Geomorphology, 392, 107915. https://doi.org/10.1016/j.geomorph.2021.107915.

544 Flint. J., 1974. Stream gradient as a function of order, magnitude, and discharge. Water Resour. Res.
545 10(5), 969-973. https://doi.org/10.1029/WR010i005p00969.

546 Forte, A.M., Yanites, B.J., Whipple, K.X., 2016. Complexities of landscape evolution during incision
547 through layered stratigraphy with contrasts in rock strength. Earth Surf. Process. Landf. 1736-
548 1757. https://doi.org/10.1002/esp.3947.

549 Forte, A.M., Whipple, K.X., 2018. Criteria and tools for determining drainage divide stability. Earth
550 Planet Sc Lett, 493, 102-117. https://doi.org/10.1016/j.epsl.2018.04.026.Gailleton, B., Mudd,
551 S.M., Clubb, F.J., Grieve, S.W.D., Hurst, M.D., 2021. Impact of changing concavity indices on
552 channel steepness and divide migration metrics. J. Geophys Res. Earth Surf. 126(10):
553 e2020JF006060. https://doi.org/10.1029/2020JF006060.

Gailleton, B., Mudd, S.M., Clubb, F.J., Peifer, D., Hurst, M.D., 2019. A segmentation approach for the reproducible extraction and quantification of knickpoints from river long profiles. Earth Surface Dynamics, 7(1), 211-230. https://doi.org/10.5194/esurf-7-211-2019.

Gallen, S.F., 2018. Lithologic controls on landscape dynamics and aquatic species evolution in post-orogenic mountains. Earth Planet Sc Lett, 493, 150-160. https://doi.org/10.1016/j.epsl.2018.04.029.

Gallen, S.F., Wegmann, K.W., Frankel, K.L., Hughes, S., Lewis, R.Q., Lyons, N., Paris, P., Ross, K., Bauer, J.B., Witt, A.C., 2011. Hillslope response to knickpoint migration in the Southern Appalachians: implications for the evolution of post‐orogenic landscapes. Earth Surf. Process. Landf. 36(9), 1254-1267. https://doi.org/10.1002/esp.2150.

Giachetta, E., Refice, A., Capolongo, D., Gasparini, N.M. and Pazzaglia, F.J., 2014. Orogen‐scale drainage network evolution and response to erodibility changes: insights from numerical experiments. Earth Surface Processes and Landforms, 39(9), 1259-1268. https://doi.org/10.1002/esp.3579.

Gilbert, G.K., 1877. Report on the Geology of the Henry Mountains. US Government Printing Office. Washington, DC.

Han, J., Gasparini, N.M., Johnson, J.P., Murphy, B.P., 2014. Modeling the influence of rainfall gradients on discharge, bedrock erodibility, and river profile evolution, with application to the Big Island, Hawai'i. J. Geophys Res. Earth Surf. 119(6), 1418-1440. https://doi.org/10.1002/2013JF002961.

Harel, M.-A., Mudd, S., Attal, M., 2016. Global analysis of the stream power law parameters based on worldwide 10Be denudation rates. Geomorphology, 268, 184-196. https://doi.org/10.1016/j.geomorph.2016.05.035.

Harkins, N., Kirby, E., Heimsath, A., Robinson, R., Reiser, U., 2007. Transient fluvial incision in the headwaters of the Yellow River, northeastern Tibet, China. J. Geophys Res. Earth Surf. 112(F3). https://doi.org/10.1029/2006JF000570.

Hartmann, J., Moosdorf, N., 2012. The new global lithological map database GLiM: A representation of rock properties at the Earth surface. Geochemistry, Geophysics, Geosystems, 13(12). https://doi.org/10.1029/2012GC004370.

He, C., Yang, C.-J., Turowski, J.M., Rao, G., Roda-Boluda, D.C., Yuan, X.-P., 2021. Constraining tectonic uplift and advection from the main drainage divide of a mountain belt. Nature communications, 12(1), 1-10. https://doi.org/10.1038/s41467-020-20748-2.

Henck, A.C., Huntington, K.W., Stone, J.O., Montgomery, D.R., Hallet, B., 2011. Spatial controls on erosion in the Three Rivers Region, southeastern Tibet and southwestern China. Earth Planet Sc Lett, 303(1-2), 71-83. https://doi.org/10.1016/j.epsl.2010.12.038.

Hergarten, S., Robl, J., Stüwe, K., 2016. Tectonic geomorphology at small catchment sizes–extensions of the stream-power approach and the χ method. Earth Surface Dynamics, 4(1), 1-9. https://doi.org/10.5194/esurf-4-1-2016.

Hurst, M.D., Grieve, S.W., Clubb, F.J., Mudd, S.M., 2019. Detection of channel-hillslope coupling along a tectonic gradient. Earth Planet Sc Lett, 522, 30-39. https://doi.org/10.1016/j.epsl.2019.06.018.

595 Kapp, P., DeCelles, P.G., 2019. Mesozoic–Cenozoic geological evolution of the Himalayan-Tibetan
596 orogen and working tectonic hypotheses. Am. J. Sci. 319, 159-254.
597 https://doi.org/10.2475/03.2019.01

598 Kirby, E., Whipple, K.X., 2012. Expression of active tectonics in erosional landscapes. Journal of
599 Structural Geology, 44, 54-75. https://doi.org/10.1016/j.jsg.2012.07.009.

600 Leonard, J.S., Whipple, K.X., 2021. Influence of Spatial Rainfall Gradients on River Longitudinal
601 Profiles and the Topographic Expression of Spatially and Temporally Variable Climates in
602 Mountain Landscapes. J. Geophys Res. Earth Surf. 126(12), e2021JF006183.
603 https://doi.org/10.1029/2021JF006183.

604 Li, J., Fang, X., Ma, H., Zhu, J., Pan, B., Chen, H., 1996. Geomorphological evolution of the upper
605 Yellow River in the Late Cenozoic and the uplift of the Qinghai-Tibet Plateau. Science in China
606 (Series D), 4, 316-322.

607 Li, Y., Wu, Z., Ye, P., Ma, D., Liu, Y., Jiang, Y., Li, J., Zhou, C., 2013. The geomorphologic and
608 geological marks of the active left-lateral strike-slip fault and the characteristics of geometry and
609 kinematics along the Yushu fault zone in southeastern Tibet. Geological Bulletin of China, 32(9),
610 1410-1422.

611 Lima, A.G., Flores, D.M., 2017. River slopes on basalts: Slope-area trends and lithologic control.
612 Journal of South American Earth Sciences, 76, 375-388.
613 https://doi.org/10.1016/j.jsames.2017.03.014.

614 Liu, Z., Han, L., Boulton, S.J., Wu, T., Guo, J., 2020. Quantifying the transient landscape response to
615 active faulting using fluvial geomorphic analysis in the Qianhe Graben on the southwest margin
616 of Ordos, China. Geomorphology, 351, 106974. https://doi.org/10.1016/j.geomorph.2019.106974.

617 Lyons, N.J., Val, P., Albert, J.S., Willenbring, J.K., Gasparini, N.M., 2020. Topographic controls on
618 divide migration, stream capture, and diversification in riverine life. Earth Surface Dynamics, 8(4),
619 893-912. https://doi.org/10.5194/esurf-8-893-2020.

620 Mandal, S.K., Lupker, M., Burg, J.-P., Valla, P.G., Haghipour, N., Christl, M., 2015. Spatial variability
621 of 10Be-derived erosion rates across the southern Peninsular Indian escarpment: A key to
622 landscape evolution across passive margins. Earth Planet Sc Lett, 425, 154-167.
623 https://doi.org/10.1016/j.epsl.2015.05.050.

624 Mitchell, N.A., Yanites, B.J., 2019. Spatially variable increase in rock uplift in the northern US
625 Cordillera recorded in the distribution of river knickpoints and incision depths. J. Geophys. Res.
626 Earth Surf. 124(5), 1238-1260. https://doi.org/10.1029/2018JF004880.

627 Molnar, P., Tapponnier, P., 1975. Cenozoic Tectonics of Asia: Effects of a Continental Collision.
628 Science 189, 419-426. https://doi.org/10.1126/science.189.4201.419

629 Morisawa, M. E., 1962. Quantitative geomorphology of some watersheds in the Appalachian Plateau.
630 Geol. Soc. Am. Bull. 73(9): 1025-1046. https://doi.org/10.1130/0016-
631 7606(1962)73[1025:QGOSWI]2.0.CO;2.

632 Mudd, S.M., Attal, M., Milodowski, D.T., Grieve, S.W.D., Valters, D.A., 2014. A statistical
633 framework to quantify spatial variation in channel gradients using the integral method of channel
634 profile analysis. J. Geophys Res. Earth Surf. 119(2), 138-152.
635 https://doi.org/10.1002/2013JF002981.

636 Mudd, S.M., Clubb, F.J., Gailleton, B., Hurst, M.D., 2018. How concave are river channels? Earth
637 Surface Dynamics, 6(2), 505-523. https://doi.org/10.5194/esurf-6-505-2018.

Nie, J., Ruetenik, G., Gallagher, K., Hoke, G., Garzione, C.N., Wang, W., Stockli, D., Hu, X., Wang, Z., Wang, Y., 2018. Rapid incision of the Mekong River in the middle Miocene linked to monsoonal precipitation. Nature Geoscience, 11(12), 944-948. https://doi.org/10.1038/s41561-018-0244-z.

Niemann, J.D., Gasparini, N.M., Tucker, G.E., Bras, R.L., 2001. A quantitative evaluation of Playfair's law and its use in testing long-term stream erosion models. Earth Surf. Process. Landf. 26(12), 1317-1332. https://doi.org/10.1002/esp.272.

Ott, R.F., 2020. How Lithology Impacts Global Topography, Vegetation, and Animal Biodiversity: A Global - Scale Analysis of Mountainous Regions. Geophys. Res. Lett., 47(20). https://doi.org/10.1029/2020GL088649.

Ou, X., Replumaz, A., van der Beek, P., 2021. Contrasting exhumation histories and relief development within the Three Rivers Region (south-east Tibet). Solid Earth, 12(3), 563-580. https://doi.org/10.5194/se-12-563-2021.

Ouimet, W., Whipple, K., Royden, L., Reiners, P., Hodges, K., Pringle, M., 2010. Regional incision of the eastern margin of the Tibetan Plateau. Lithosphere, 2(1), 50-63. https://doi.org/10.1130/L57.1.

Ouimet, W.B., Whipple, K.X., Granger, D.E., 2009. Beyond threshold hillslopes: Channel adjustment to base-level fall in tectonically active mountain ranges. Geology, 37(7), 579-582. https://doi.org/10.1130/G30013A.1.

Ouimet, W. B., 2007. Dissecting the eastern margin of the Tibetan Plateau: A study of landslides, erosion and river incision in a transient landscape (Doctoral dissertation). Massachusetts Institute of Technology.

Pan, B., Wang, Z., Li, Z., Yu, G.-a., Xu, M., Zhao, N., Brierley, G., 2013. An exploratory analysis of benthic macroinvertebrates as indicators of the ecological status of the Upper Yellow and Yangtze Rivers. Journal of Geographical Sciences, 23(5), 871-882. Https://doi.org/10.1007/s11442-013-1050-6.

Perron, J.T., Royden, L., 2013. An integral approach to bedrock river profile analysis. Earth Surf. Process. Landf. 38(6), 570-576. https://doi.org/10.1002/esp.3302.

Roering, J.J., Kirchner, J.W., Dietrich, W.E., 1999. Evidence for nonlinear, diffusive sediment transport on hillslopes and implications for landscape morphology. Water Resour. Res. 35(3), 853-870. https://doi.org/10.1029/1998WR900090.

Roering, J.J., Kirchner, J.W., Dietrich, W.E., 2001. Hillslope evolution by nonlinear, slope-dependent transport: Steady state morphology and equilibrium adjustment timescales. J. Geophys Res. Earth Surf. 106(B8), 16499-16513. https://doi.org/10.1029/2001JB000323.

Roering, J.J., Perron, J.T., Kirchner, J.W., 2007. Functional relationships between denudation and hillslope form and relief. Earth Planet Sc Lett, 264(1-2), 245-258. https://doi.org/10.1016/j.epsl.2007.09.035.

Roger, F., Malavieille, J., Leloup, P.H., Calassou, S., Xu, Z., 2004. Timing of granite emplacement and cooling in the Songpan–Garzê Fold Belt (eastern Tibetan Plateau) with tectonic implications. Journal of Asian Earth Sciences, 22(5), 465-481. https://doi.org/10.1016/S1367-9120(03)00089-0.

679 Royden, L.H., Burchfiel, B.C., King, R.W., Wang, E., Chen, Z., Shen, F., Liu, Y., 1997. Surface
680 deformation and lower crustal flow in eastern Tibet. Science, 276(5313), 788-790.
681 https://doi.org/10.1126/science.276.5313.788.

682 Safran, E.B., Bierman, P.R., Aalto, R., Dunne, T., Whipple, K.X., Caffee, M., 2005. Erosion rates
683 driven by channel network incision in the Bolivian Andes. Earth Surf. Process. Landf. 30(8),
684 1007-1024. https://doi.org/10.1002/esp.1259.

685 Scherler, D., Bookhagen, B., Strecker, M.R., 2014. Tectonic control on 10Be-derived erosion rates in
686 the Garhwal Himalaya, India. J. Geophys. Res. Earth Surf. 119(2), 83-105.
687 https://doi.org/10.1002/2013JF002955.

688 Searle, M.P., Roberts, N.M., Chung, S.-L., Lee, Y.-H., Cook, K.L., Elliott, J.R., Weller, O.M., St-Onge,
689 M.R., Xu, X.-W., Tan, X.-B., 2016. Age and anatomy of the Gongga Shan batholith, eastern
690 Tibetan Plateau, and its relationship to the active Xianshui-he fault. Geosphere 12, 948-970.
691 https://doi.org/10.1130/GES01244.1.

692 Shen, X., Tian, Y., Li, D., Qin, S., Vermeesch, P. and Schwanethal, J., 2016. Oligocene-Early Miocene
693 river incision near the first bend of the Yangze River: Insights from apatite (U-Th-Sm)/He
694 thermochronology. Tectonophysics, 687: 223-231. https://doi.org/10.1016/j.tecto.2016.08.006

695 Snyder, N.P., Whipple, K.X., Tucker, G.E., Merritts, D.J., 2000. Landscape response to tectonic
696 forcing: Digital elevation model analysis of stream profiles in the Mendocino triple junction
697 region, northern California. Geol. Soc. Am. Bull. 112(8), 1250-1263.
698 https://doi.org/10.1130/0016-7606(2000)112<1250:LRTTFD>2.0.CO;2.

699 Souza, M.S., Thomaz, A.T., Fagundes, N.J., 2020. River capture or ancestral polymorphism: an
700 empirical genetic test in a freshwater fish using approximate Bayesian computation. Biological
701 Journal of the Linnean Society, 131(3), 575-584. https://doi.org/10.1093/biolinnean/blaa140.

702 Spicer R. A., 2017. Tibet, the Himalaya, Asian monsoons and biodiversity–In what ways are they
703 related?. Plant Diversity, 2017, 39(5): 233-244. https://doi.org/10.1016/j.pld.2017.09.001.

704 Spurlin, M.S., Yin, A., Horton, B.K., Zhou, J., Wang, J., 2005. Structural evolution of the Yushu-
705 Nangqian region and its relationship to syncollisional igneous activity, east-central Tibet. Geol.
706 Soc. Am. Bull. 117, 1293-1317. https://doi.org/10.1130/B25572.1.

707 Strong, C.M., Attal, M., Mudd, S.M., Sinclair, H.D., 2019. Lithological control on the geomorphic
708 evolution of the Shillong Plateau in Northeast India. Geomorphology, 330, 133-150.
709 https://doi.org/10.1093/nsr/nwaa091.

710 Struth, L., Garcia-Castellanos, D., Viaplana-Muzas, M., Vergés, J., 2019. Drainage network dynamics
711 and knickpoint evolution in the Ebro and Duero basins: From endorheism to exorheism.
712 Geomorphology, 327, 554-571. https://doi.org/10.1016/j.geomorph.2018.11.033.

713 Studnicki-Gizbert, C., Burchfiel, B., Li, Z., Chen, Z., 2008. Early Tertiary Gonjo basin, eastern Tibet:
714 Sedimentary and structural record of the early history of India-Asia collision. Geosphere, 4(4),
715 713-735. https://doi.org/10.1130/GES00136.1.

716 Swartz, E.R., Skelton, P.H., Bloomer, P., 2007. Sea-level changes, river capture and the evolution of
717 populations of the Eastern Cape and fiery redfins (Pseudobarbus afer and Pseudobarbus
718 phlegethon, Cyprinidae) across multiple river systems in South Africa. Journal of Biogeography,
719 34(12), 2086-2099. https://doi.org/10.1111/j.1365-2699.2007.01768.x.

Takaku, J., Tadono, T., Tsutsui, K., 2014. Generation of high resolution global DSM from Alos Prism. ISPRS Annals of Photogrammetry, Remote Sensing & Spatial Information Sciences, 2(4). https://doi.org/10.5194/isprsarchives-XL-4-243-2014.

Taylor, M., Yin, A., 2009. Active structures of the Himalayan-Tibetan orogen and their relationships to earthquake distribution, contemporary strain field, and Cenozoic volcanism. Geosphere, 5(3), 199-214. https://doi.org/10.1130/GES00217.1.

Tian, Y., Kohn, B.P., Gleadow, A.J.W. and Hu, S., 2014. A thermochronological perspective on the morphotectonic evolution of the southeastern Tibetan Plateau. J. Geophys. Res. Solid Earth, 119(1): 676-698. https://doi.org/10.1002/2013JB010429.

Tian, Y., Li, R., Tang, Y., Xu, X., Wang, Y. and Zhang, P., 2018. Thermochronological Constraints on the Late Cenozoic Morphotectonic Evolution of the Min Shan, the Eastern Margin of the Tibetan Plateau. Tectonics, 37(6): 1733-1749. https://doi.org/10.1029/2017TC004868.

Tucker, G. E., Whipple, K. X., 2002. Topographic outcomes predicted by stream erosion models: Sensitivity analysis and intermodel comparison. J. Geophys. Res. Solid Earth, 107(B9), ETG 1-1-ETG 1-16. https://doi.org/10.1029/2001JB000162.

van Hinsbergen, D.J.J., Lippert, P.C., Dupont-Nivet, G., McQuarrie, N., Doubrovine, P.V., Spakman, W., Torsvik, T.H., 2012. Greater India Basin hypothesis and a two-stage Cenozoic collision between India and Asia. Proc. Nat. Acad. Sci. 109, 7659-7664. https://doi.org/10.1073/pnas.1117262109.

VanLaningham, S., Meigs, A., Goldfinger, C., 2006. The effects of rock uplift and rock resistance on river morphology in a subduction zone forearc, Oregon, USA. Earth Surf. Process. Landf. 31(10), 1257-1279. https://doi.org/10.1002/esp.1326.

Wang, C., Zhao, X., Liu, Z., Lippert, P.C., Graham, S.A., Coe, R.S., Yi, H., Zhu, L., Liu, S., Li, Y., 2008. Constraints on the early uplift history of the Tibetan Plateau. Proc. Natl. Acad. Sci. U. S. A. 105(13): 4987-4992.

Wang, E., Burchfiel, B.C., 2000. Late Cenozoic to Holocene deformation in southwestern Sichuan and adjacent Yunnan, China, and its role in formation of the southeastern part of the Tibetan Plateau. Geol. Soc. Am. Bull. 112(3), 413-423. https://doi.org/10.1130/0016-7606(2000)112<413:LCTHDI>2.0.CO;2.

Wang, E., Kirby, E., Furlong, K.P., van Soest, M., Xu, G., Shi, X., Kamp, P.J.J. and Hodges, K.V., 2012. Two-phase growth of high topography in eastern Tibet during the Cenozoic. Nature Geosci, 5(9): 640-645. https://doi.org/10.1138/NGEO1538.

Wang, S., Fan, C., Wang, G., Wang, E., 2008. Late Cenozoic deformation along the northwestern continuation of the Xianshuihe fault system, Eastern Tibetan Plateau. Geol. Soc. Am. Bull. 120(3-4), 312-327. https://doi.org/10.1130/B25833.1.

Waters, J.M., Burridge, C.P., Craw, D., 2020. River Capture and Freshwater Biological Evolution: A Review of Galaxiid Fish Vicariance. Diversity, 12(6), 216. https://doi.org/10.3390/d12060216.

Wen, X., Huang, S., Jiang, Z., 1985. Neotectonic characteristics and seismic risk assessment of the Ganzi-Yushu fault zone. Seismology and Geology, 7(3), 23-32.

Wen, X., Xun, X., Zheng, R., 2003. The average slip rae of Ganzi-Yushu fault and the fragmentation of mordern earthquake. Science in China (Series D), 33(1), 199-208. https://doi.org/10.3969/j.issn.1674-7240.2003.z1.022.

Whipple, K.X., 2001. Fluvial landscape response time: How plausible is steady-state denudation? American Journal of Science, 301(4-5), 313-325. https://doi.org/10.2475/ajs.301.4-5.313.

Whipple, K.X., DiBiase, R.A., Ouimet, W.B., Forte, A.M., 2017a. Preservation or piracy: Diagnosing low-relief, high-elevation surface formation mechanisms. Geology, 45(1), 91-94. https://doi.org/10.1130/G38490.1.

Whipple, K.X., Forte, A.M., Dibiase, R.A., Gasparini, N.M., Ouimet, W.B., 2017b. Timescales of landscape responseto divide migration and drainage capture: Implications for the role of divide mobility in landscape evolution. J. Geophys. Res. Earth Surf. 122, 248–273. https://doi.org/10.1002/2016JF003973

Whipple, K.X., Kirby, E., Brocklehurst, S.H., 1999. Geomorphic limits to climate-induced increases in topographic relief. Nature, 401(6748), 39-43. https://doi.org/10.1038/43375.

Whipple, K.X., Tucker, G.E., 1999. Dynamics of the stream-power river incision model: Implications for height limits of mountain ranges, landscape response timescales, and research needs. J. Geophys. Res. Solid Earth, 104(B8), 17661-17674. https://doi.org/10.1029/1999JB900120.

Whittaker, A.C., Boulton, S.J., 2012. Tectonic and climatic controls on knickpoint retreat rates and landscape response times. J. Geophys. Res. Earth Surf. 117(F2). https://doi.org/10.1029/2011JF002157.

Wickert, A.D., Schildgen, T.F., 2019. Long-profile evolution of transport-limited gravel-bed rivers. Earth Surface Dynamics, 7(1), 17-43. https://doi.org/10.5194/esurf-7-17-2019.

Willett, S.D., Mccoy, S.W., Perron, J.T., Goren, L., Chen, C.Y., 2014. Dynamic Reorganization of River Basins. Science, 343(6175), 1117-1117. https://doi.org/10.1126/science.1248765.

Wilson, C.J., Fowler, A.P., 2011. Denudational response to surface uplift in east Tibet: Evidence from apatite fission-track thermochronology. Geol. Soc. Am. Bull. 123(9-10), 1966-1987. https://doi.org/10.1130/B30331.1.

Wobus, C., Whipple, K.X., Kirby, E., Snyder, N., Johnson, J., Spyropolou, K., Crosby, B., Sheehan, D., Willett, S., 2006. Tectonics from topography: Procedures, promise, and pitfalls. Geol. Soc. Am. Bull. 398, 55. https://doi.org/10.1130/2006.2398(04).

Yang, R., Willett, S.D., Goren, L., 2015. In situ low-relief landscape formation as a result of river network disruption. Nature, 520(7548), 526-529. https://doi.org/10.1038/nature14354.

Yin, A., Harrison, T.M., 2000. Geologic Evolution of the Himalayan-Tibetan Orogen. Annual Review of Earth and Planetary Sciences 28, 211-280. https://doi.org/10.1146/annurev.earth.28.1.211.

Yu, Y., Wang, X., Li, Y., Dai, Y., Lu, H., 2018. The evolution of drainage pattern and its relation to tectonic movement in the upstream Yangtze catchment. Acta Geographica Sinica, 73(7), 1338-1350. https://doi.org/10.11821/dlxb201807012.

Yu, Y., Wang, X., Yi, S., Miao, X., Vandenberghe, J., Li, Y., Lu, H., 2021. Late Quaternary aggradation and incision in the headwaters of the Yangtze River, eastern Tibetan Plateau, China. Geol. Soc. Am. Bull. 134(1-2): 371-388. https://doi.org/10.1130/B35983.1.

Yuan, X., Huppert, K. L., Braun, J., Shen, X., Zeng, L., Guerit, L., Wolf, S. G., Zhang, J., Jolivet, M., 2022. Propagating uplift controls on high-elevation, low-relief landscape formation in the southeast Tibetan Plateau. Geology, 2022, 50(1): 60-65. https://doi.org/10.1130/G49022.1.

Zhang, G., Tian, Y., Li, R., Shen, X., Zhang, Z., Sun, X. and Chen, D., 2022. Progressive tectonic evolution from crustal shortening to mid-lower crustal expansion in the southeast Tibetan Plateau: A synthesis of structural and thermochronological insights. Earth-Science Reviews, 226: 103951. https://doi.org/10.1016/j.earscirev.2022.103951.

Zhang, Y., Yao, X., Zhou, S., Zhang, D., 2021. A glacier vector dataset in the Three-River Headwaters region during 2000-2019. Science Data Bank. https://www.dx.doi.org/10.11922/sciencedb.j00001.00234.

Zhou, R., Wen, X., Chai, C., 1997. Recent earthquakes and assessment of seismic tendency on the Ganzi-Yushu fault zone. Seismology and Geology, 19(2), 115-124.

Zondervan, J.R., Whittaker, A.C., Bell, R.E., Watkins, S.E., Brooke, S.A. and Hann, M.G., 2020a. New constraints on bedrock erodibility and landscape response times upstream of an active fault. Geomorphology, 351:106937. https://doi.org/10.1016/j.geomorph.2019.106937.

Zondervan, J.R., Stokes, M., Boulton, S.J., Telfer, M.W. and Mather, A.E., 2020b. Rock strength and structural controls on fluvial erodibility: Implications for drainage divide mobility in a collisional mountain belt. Earth and Planetary Science Letters, 538, 116221. https://doi.org/10.1016/j.epsl.2020.116221.

821 Supplimentary material

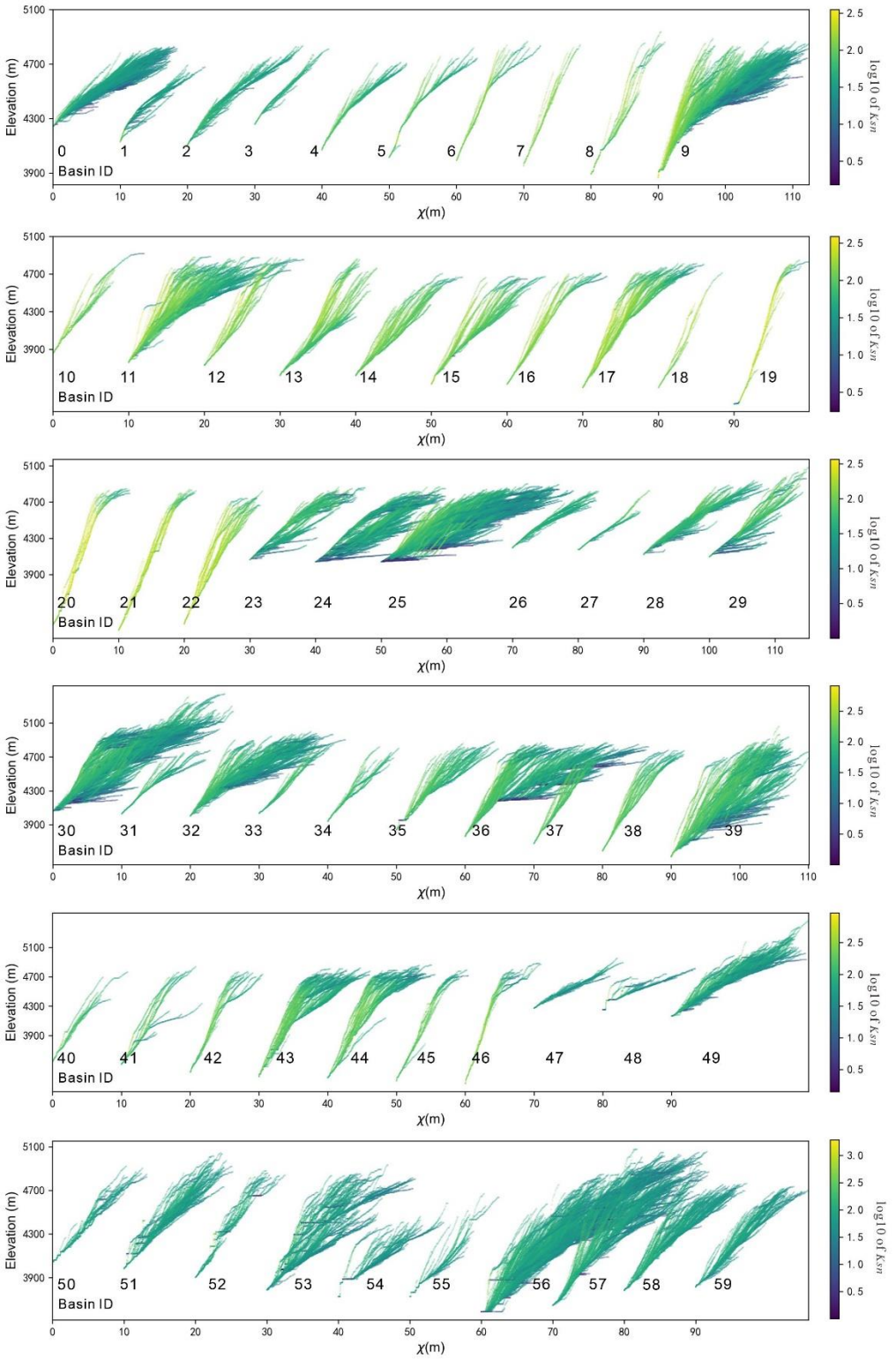

Figure 1. χ plots of all catchments analyzed. Basin ID corresponds to Figure 1-b.

822